frontiers in Energy Research

ORIGINAL RESEARCH
published: 28 July 2016
doi: 10.3389/fenrg.2016.00030

Grain Boundary Analysis of the Garnet-Like Oxides $Li_{7+X-Y}La_{3-X}A_XZr_{2-Y}Nb_YO_{12}$ (A = Sr or Ca)

Shingo Ohta, Yuki Kihira and Takahiko Asaoka*

Battery & Cell Division, Toyota Central R&D Labs. Inc., Nagakute, Japan

Garnet-like oxides having the formula $Li_{7+X-Y}La_{3-X}A_XZr_{2-Y}Nb_YO_{12}$ (A = Sr or Ca) were synthesized using a solid-state reaction, and their bulk and grain boundary resistivities were assessed by AC impedance measurements. A difference in grain boundary resistivity was identified between Sr and Ca materials, and so the grain boundaries were examined using electron probe microanalysis (EPMA). The difference in the grain boundary resistivities was attributed to the core–shell structure of the Sr-substituted samples. In contrast, the Ca-substituted materials exhibited accumulations of impurities at the grain boundaries.

Keywords: solid electrolytes, oxide, ion conductivity, grain boundary, all-solid-state, lithium ion battery

OPEN ACCESS

Edited by:
Shyue Ping Ong,
University of California,
San Diego, USA

Reviewed by:
Liqiang Mai,
Wuhan University of Technology,
China
Lincoln James Miara,
Samsung Electronics America,
Inc. (SEA)

****Correspondence:***
Shingo Ohta
shingo_ohta@mail.toyota.co.jp,
sohta@mosk.tytlabs.co.jp

Specialty section:
This article was submitted to Energy Storage, a section of the journal Frontiers in Energy Research

Received: *30 January 2016*
Accepted: *11 July 2016*
Published: *28 July 2016*

Citation:
Ohta S, Kihira Y and Asaoka T (2016) Grain Boundary Analysis of the Garnet-Like Oxides $Li_{7+X-Y}La_{3-X}A_XZr_{2-Y}Nb_YO_{12}$ (A = Sr or Ca). Front. Energy Res. 4:30. doi: 10.3389/fenrg.2016.00030

INTRODUCTION

It is increasingly important to ensure the safety of lithium ion batteries as they are considered for use as power sources in electric vehicles or airplanes. These batteries typically use flammable organic liquids as the electrolyte, and so to improve the safety of lithium ion batteries, solid-state electrolytes have been developed to allow the fabrication of incombustible all-solid-state devices. Solid oxide electrolytes are believed to potentially have advantages over other inorganic electrolytes, such as sulfides, in terms of their chemical stability and lack of toxic degradation products (Ohtomo et al., 2013a,b). The garnet-like oxide $Li_7La_3Zr_2O_{12}$ (LLZ), which was reported by Prof. Murugan in 2007, is one of the most promising oxide electrolytes because of its excellent lithium ion conductivity ($\geq 10^{-4}$ Scm^{-1}) and wide potential window (Murugan et al., 2007). Following the discovery of LLZ, there were extensive efforts to improve its lithium ion conductivity, especially by elemental substitution leading to structural modification of the framework atoms (Rangasamy et al., 2013; Jalem et al., 2013; Thompson et al., 2014). This substitution modifies the lithium ion pathway by varying the bulk lithium ion conductivity, and many researchers have focused on improving the bulk lithium ion conductivity of garnet as a means of enhancing the conductivity of LLZ (Nyman et al., 2010; Ohta et al., 2011; Logeat et al., 2012; Allen et al., 2012). However, practical all-solid-state lithium ion batteries are likely to be fabricated by typical solid-state reactions, such that the primary contributor to the internal resistance of the solid oxide electrolyte will not be the bulk resistance, but rather the grain boundary resistivity (R_{gb}) of the polycrystalline electrolyte. As such, the total resistivity (R_{total}) of the electrolyte, including the R_{gb}, is important. Generally, the grain boundary resistance of a solid oxide electrolyte is high, meaning that the total ion conductivity has almost the same value as the grain boundary ion conductivity. Lithium lanthanum titanate, for example, is known to exhibit high ionic conductivity along with a high bulk conductivity of $\sigma_{bulk} = 1 \times 10^{-3}$ Scm^{-1}. However, the two-dimensional lithium ion paths in this material are interrupted by grain boundaries, resulting in a high R_{gb} with $\sigma_{grain\ boundary} \approx \sigma_{total} = 2 \times 10^{-5}$ Scm^{-1} (Inaguma et al., 1993; Stramare et al., 2003;

Yashima et al., 2005; Gao et al., 2014; Moriwake et al., 2015). In contrast, the grain boundary resistance of garnet-like oxides is relatively low compared to other ion-conducting oxides because of the good lithium ion connection between grains, forming three dimensional lithium ion paths. These materials thus show total lithium ion conductivity values as high as the bulk lithium ion conductivity (that is, $\sigma_{total} \approx \sigma_{bulk}$) (Ohta et al., 2011; Allen et al., 2012). However, the R_{gb} values of garnet-like oxides vary widely, from several percent to 40% of the R_{total}, depending on the composition (Li et al., 2012; Kihira et al., 2013). These differences in R_{gb} are believed to arise from the effects of substances at the grain boundaries. For this reason, the grain boundary resistivities induced by substitution with other elements should be assessed as a means of minimizing the R_{gb} and to determine the optimum substitution elements for garnet-like oxides.

In the present study, we simultaneously made substitutions at both the Zr and La sites to synthesize $Li_{7+X-Y}(La_{3-X}A_X)(Zr_{2-Y}Nb_Y)O_{12}$ (A-LLZNb; A = Ca, Sr). This was done to determine the optimum composition with regard to obtaining the highest lithium ion conductivity, based on differences in valency and ionic size: Nb^{5+} (0.64 Å), Zr^{4+} (0.72 Å), Ca^{2+} (1.34 Å), La^{3+} (1.36 Å), and Sr^{2+} (1.44 Å) (Shannon, 1976). Through these investigations, we found that the R_{gb} showed different characteristics between Ca and Sr substitutions. This study clarified that the ionic size and valency of the substitution element affect the grain and grain boundary morphology, and consequently the total lithium ion conductivity. This effect is discussed herein based on the grain boundaries of A-LLZNb incorporating Sr and Ca, as assessed *via* electron probe microanalysis (EPMA).

MATERIALS AND METHODS

$Li_{7+X-Y}(La_{3-X}A_X)(Zr_{2-Y}Nb_Y)O_{12}$ (A-LLZNb; A = Ca or Sr) bulk ceramic samples were synthesized by a conventional solid-state reaction in alumina crucibles. The starting materials were Li_2CO_3 (a 10% excess was added to allow for lithium losses by evaporation at high temperatures), $La(OH)_3$, ZrO_2, Nb_2O_5, and alkali earth metals in the form of carbonates.

The electrical conductivity of each sample was measured in air using a two-probe AC impedance method with an Agilent 4294A instrument over the frequency range of 110 MHz to 40 Hz at 25°C. Au electrodes were applied to both sides of the sample pellets using Au paste prior to these measurements, and the pellet and paste were subsequently annealed at 800°C for 0.5 h. The morphologies and the elemental distributions of the Ca or Sr-LLZNb bulk ceramics were measured by EPMA (JEOL Ltd. JXA-8500F). The crystal structures and impurity phases of the samples were determined by X-ray diffraction (XRD, Rigaku Co., Ltd., Ultima IV) using Cu Kα radiation.

RESULTS AND DISCUSSION

Figure 1 shows the AC impedance plots (Nyquist plots) of the synthesized A-LLZNb (A = Sr or Ca) bulk ceramic samples, where a = $Li_7La_2Sr_1Zr_1Nb_1O_{12}$ (1.0Sr-LLZNb), b = $Li_7La_{2.25}Ca_{0.75}Zr_{1.25}Nb_{0.75}O_{12}$ (0.75Ca-LLZNb), and c = $Li_7La_2Ca_1Zr_1Nb_1O_{12}$ (1.0Ca-LLZNb). When analyzing the impedance plot of a garnet oxide, there will be two semi-circles indicating the bulk resistivity (R_{bulk}) at higher frequencies (each terminal frequencies are 0.3M ~ 0.1 MHz) and the R_{gb} at lower frequencies (each terminal frequencies are 5000 ~ 50 Hz), the sum of which results in the R_{total}. The R_{bulk} and R_{gb} of the A-LLZNb (A = Sr or Ca) specimens are listed in **Table 1**. The R_{bulk} values and terminal frequencies of all samples were almost similar (~10^3 Ωcm and ~0.1 MHz), indicating that the R_{bulk} was not significantly affected by the substitution element. In contrast, the R_{gb} values of samples a, b, and c demonstrate that the substitution element makes a large difference with regard to the R_{gb} range. Each terminal frequencies are different by two orders of magnitude (5000 ~ 50 Hz). As shown in **Figure 1D**, the R_{gb} to R_{total} ratio in the Sr-LLZNb series increased gradually upon elevating the substitution level. In contrast, the ratios of the Ca-LLZNb series remained low until the substitution level reached 0.75, after which the ratio value increased significantly, eventually becoming quite large at higher substitution levels. These results suggest three discussion points: (i) the cause of the sudden jump in the R_{gb} values of the Ca-LLZNb series, (ii) the reason for the gradual increase in the R_{gb} values of the Sr-LLZNb series upon adding more Sr and Nb, and (iii) the reason why the R_{gb} values of the Sr-LLZNb series are higher than those of the Ca-LLZNb. In order to clarify the above points, we investigated the morphologies at grain boundaries and the relationship between these morphologies and composition, using EPMA.

Figure 2A shows the Ca, Al, La, Zr, and Nb EPMA maps obtained from a 0.75Ca-LLZNb sample. Al was not a constituent element but was identified as a contaminant in the sample, likely originating from the Al_2O_3 crucible during the sintering process, and so the Al distribution was assessed. The linear analysis results obtained along the red line in the back scattered electron (BSE) map in **Figure 2A** are provided in **Figure 2B**. The distributions of the elements and the linear analysis results indicate that Al and Ca were located at the grain boundary triple points in the sample. In contrast, no segregation and no elemental concentration gradients were observed in garnet grains, suggesting that the composition of the garnet grains was uniform. In order to clarify the composition of the impurity in the Ca-LLZNb series, XRD patterns were acquired, as shown in **Figure 2C**. The Ca-LLZNb for which $X < 0.5$ generated only diffraction peaks corresponding to the garnet phase, indicating that a small amount of Ca can be substituted at the La sites. Conversely, impurity peaks assigned to CaO, $LiAlO_2$, and $CaAl_2O_4$ were produced by heavily Ca-substituted samples ($X \geq 0.5$). Thus, the solid solubility limit of Ca in LLZNb appears to coincide with an X value of ~0.5, after

TABLE 1 | R_{bulk} and R_{gb} values of the A-LLZNb (A = Sr or Ca, X = 0.25, 0.5, 0.75, or 0.1) series.

	$Li_7(La_{3-X}Ca_X)(Zr_{2-X}Nb_X)_{12}$		$Li_7(La_{3-X}Sr_X)(Zr_{2-X}Nb_X)_{12}$	
	R_{buik} (Ω)	R_{gb} (Ω)	R_{buik} (Ω)	R_{gb} (Ω)
X = 0.25	2.1×10^3	2.7×10^2	8.5×10^3	1.4×10^3
X = 0.5	3.4×10^3	1.8×10^2	5.2×10^3	1.9×10^3
X = 0.75	5.8×10^3	2.5×10^2	5.3×10^3	4.6×10^3
X = 0.1	2.7×10^4	2.7×10^5	7.5×10^3	1.0×10^4

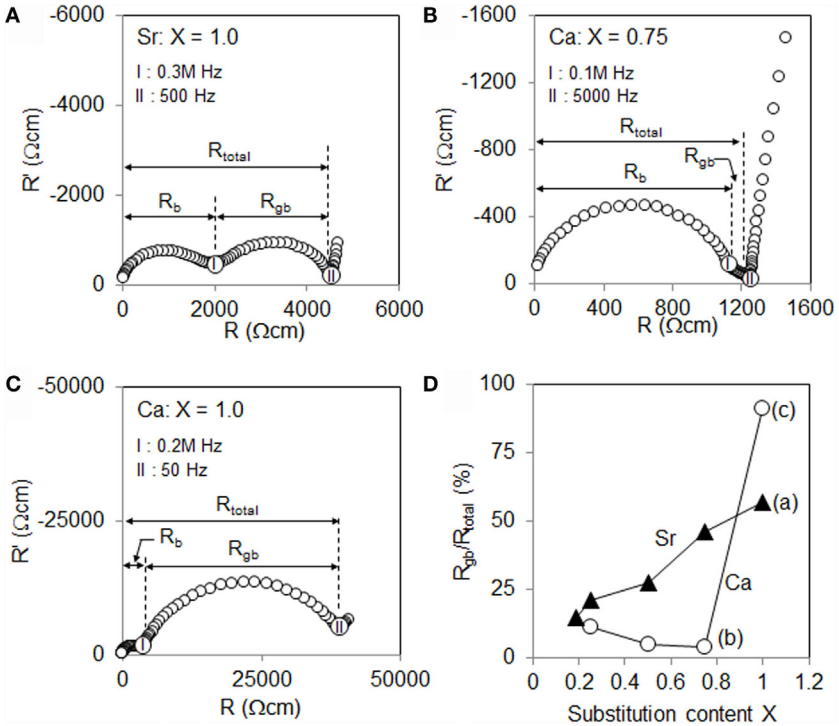

FIGURE 1 | **Nyquist plots for Li_{7+X-Y} $(La_{3-X}A_X)(Zr_{2-Y}Nb_Y)O_{12}$ (A-LLZNb, A = Sr or Ca) in which (A) A = Sr, *X* = 1.0, (B) A = Ca, *X* = 0.75, (C) A = Ca, *X* = 1.0, and (D) the ratios of resistance due to grain boundaries to total resistance (R_{gb}/R_{total}) as functions of *X***. The terminal frequencies of both resistances are shown in the graph.

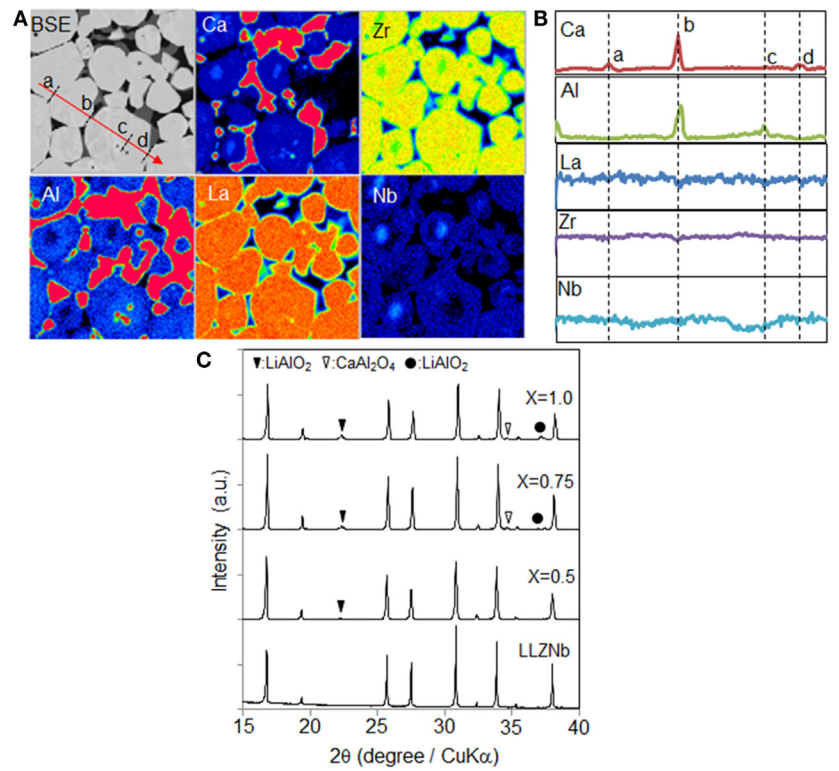

FIGURE 2 | **(A)** Cross-sectional EPMA mapping images of Ca-LLZNb, **(B)** linear analysis of Ca, Al, La, Zr, and Nb, and **(C)** XRD pattern obtained from Ca-LLZNb.

which the excess Ca accumulates at the grain boundaries. Based on this finding, an Al introduction mechanism can be proposed. In this mechanism, disproportionation of the garnet phase is induced upon the addition of Ca in excess of its solubility limit, after which excess Ca and Li accumulate at the grain boundaries. The excess Li reacts with the Al_2O_3 crucible such that Al is introduced into the sample, and $LiAlO_2$ and $CaAl_2O_4$ are subsequently formed during the sintering process.

Figure 3A presents the Sr, Al, La, Zr, and Nb EPMA maps generated by the 1.0Sr-LLZNb sample, while the linear analysis results obtained along the red line in the BSE map in **Figure 3A** are shown in **Figure 3B**. The garnet grains were determined to have a core–shell structure. The line scans show that, within the shell region and close to the grain boundaries at points a, b, c, and d in the BSE map in **Figure 3A**, there were higher concentrations of Sr and Nb and lower concentrations of La and Zr compared to the core region. Although the segregation of both Sr and Zr was observed in this field of view, $SrZrO_3$ diffraction peaks were not detected by XRD (**Figure 3C**). This result would suggest that the concentration of $SrZrO_3$ as an impurity was very low, and so we believe that the solubility limit of Sr in LLZNb is high compared to that of Ca. Al appears to have diffused into the grain boundaries of the sample from the Al_2O_3 crucible during sintering just as in the case of the Ca-LLZNb. A mechanism for this Al introduction can be proposed based on elemental distribution analysis, since this analysis found that there was an elemental concentration gradient inside the Sr-LLZNb grains. It thus appears that $LiAlO_2$ formation was induced by Li release due to structural disorder, just as is thought to have occurred with the Ca-LLZNb.

The elemental distribution and linear analysis results clearly show that the state of the grains and grain boundaries result from the effects of Sr or Ca substitution in the LLZNb. **Figure 4** presents schematic images of the grains and grain boundaries of Ca- or Sr-substituted LLZNb that appear at different R_{gb} ratios. Based on these schematics, we propose a reason for the gradual increase in the R_{gb} value of Sr-LLZNb with increasing Sr content. As greater amounts of Sr are added, the Sr will be forced out toward the boundaries to form a Sr-rich layer. The ionic radius of Sr^{2+} (1.44 Å) is greater than that of La^{3+} (1.36 Å), and their valence numbers are also different, and so the appearance of the Sr-rich layer must be balanced through an adjustment of both the structure and valency to form a garnet structure. Interestingly, Nb^{5+} (0.64 Å), which has a smaller ionic radius than Zr^{4+} (0.72 Å), and whose valence number is larger rather than smaller (as is the case with Sr^{2+} and La^{3+}), allows a balance to be maintained such that the Sr-rich garnet structure is unchanged (**Table 2**). Hence, although the solid solubility limit of Sr in LLZNb is higher than that of Ca, the gradual increase in the R_{gb} ratio in the Sr-LLZNb series is attributed to a Sr,Nb-rich layer that becomes increasingly thick as the amount of Sr added is increased (**Figures 4A,B**).

It is also possible to explain the lower solid solubility limit of Ca in LLZNb compared to that of Sr. The ionic radii of both Ca^{2+} (1.34 Å) and Nb^{5+} (0.64 Å) are smaller than those of La^{3+} (1.36 Å) and Zr^{4+} (0.72 Å), so the garnet structure cannot be

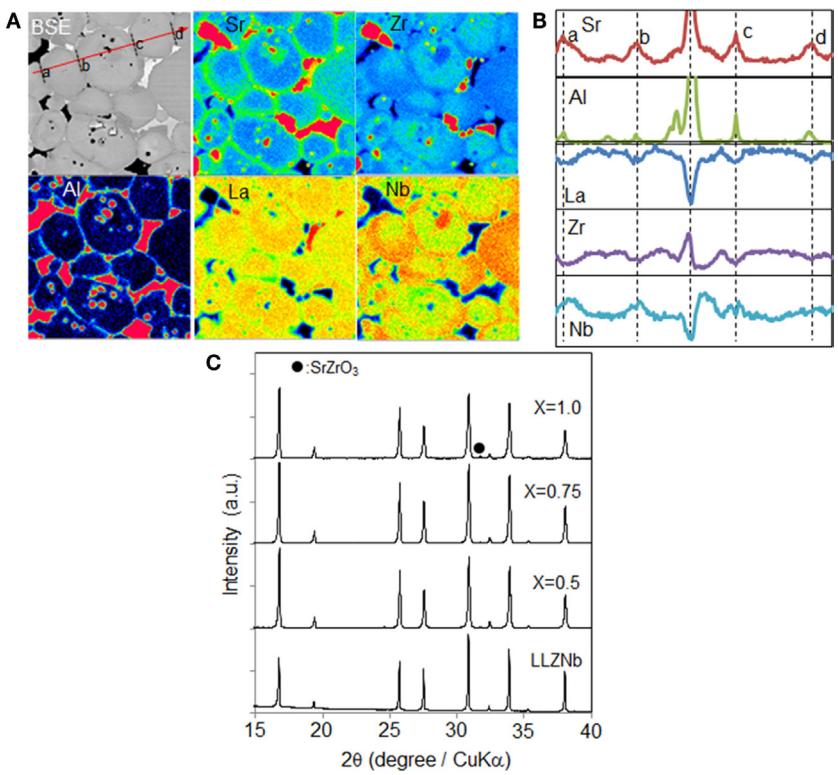

FIGURE 3 | **(A)** Cross-sectional EPMA mapping images of Sr-LLZNb, **(B)** linear analysis of Sr, Al, La, Zr, and Nb, and **(C)** XRD pattern obtained from Sr-LLZNb.

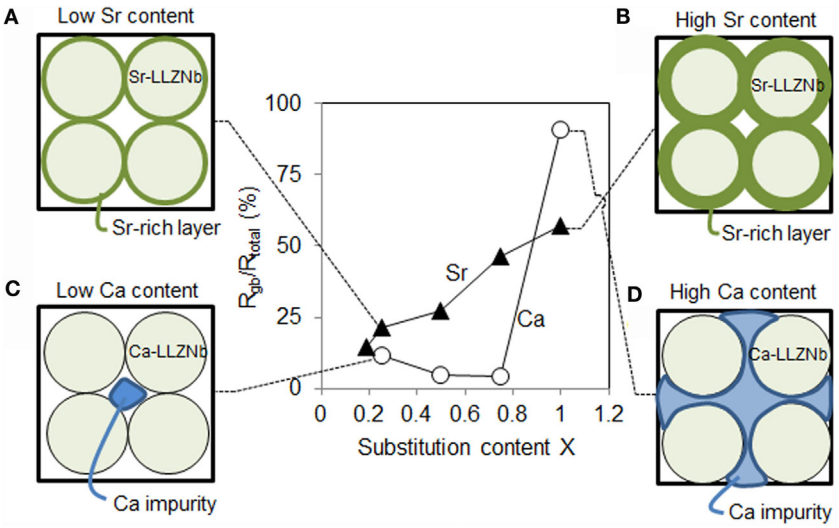

FIGURE 4 | Schematic images of the grains and grain boundaries of (A) low Sr and (B) high Sr-substituted LLZNb, and (C) low Ca and (B) high Ca-substituted LLZNb. (D) R_{gb}/R_{total} ratios as functions of *X*.

TABLE 2 | Valence numbers and ionic radii of elements substituted into the A-LLZNb (A = Sr or Ca) series.

	Sr-LLZN						Ca-LLZN					
	La site			ZR site			La site			ZR site		
	La		Sr	Zr		Nb	La		Ca	Zr		Nb
Charge	3+	down →	2+	4+	up →	5+	3+	down →	2+	4+	up →	5+
Radii	1.36	up →	1.44	0.72	down →	0.64	1.36	down →	1.34	0.72	down →	0.64

adjusted, although the relationship of their valance number is same as is possible in the case of Sr-LLZNb (**Table 2**). When the Ca substitution level is close to the solid solubility limit, although small amounts of Ca and Al impurities are accumulated at the grain boundary triple points, a Li conduction pathway can form due to sufficient contact between grains, such that the R_{gb} of the LLZNb remains low (**Figure 4C**). When the Ca substitution level is above the solid solubility limit, significant concentrations of Ca and Al impurities are accumulated at the grain boundaries, leading to insufficient contact between grains (**Figure 4D**). This is the reason why the R_{gb} of the LLZNb suddenly increases when high concentrations of Ca are substituted.

CONCLUSION

We successfully fabricated Li_{7+X-Y} $(La_{3-X}A_X)(Zr_{2-Y}Nb_Y)O_{12}$ (A-LLZNb; A = Ca, Sr) by solid-state reaction. The observed variations in the R_{gb} ratio between Sr-LLZNb and Ca-LLZNb are considered to result from the different substitution elements. Three issues were addressed in this work: (i) the sudden jump in the R_{gb} values of the Ca-LLZNb series, (ii) the higher R_{gb} values of the Sr-LLZNb series, and (iii) the gradual increase in the R_{gb} values of the Sr-LLZNb upon adding increasing amounts of Sr and Nb.

With regard to issue (i), EPMA analysis found Ca and Al at the grain boundaries of the Ca-LLZNb at $X = 1.0$, explaining the very high R_{gb} ratio. Point (ii) was elucidated by results showing a Sr,Nb-rich layer on the surfaces of garnet grains. The effect in point (iii) is thought to result from this Sr,Nb-rich layer, which would be balanced by variations in ionic size and valence. In the case of Sr-Nb or Ca-Nb combinations, the larger Sr^{2+} ions at the La^{3+} sites would be balanced by smaller Nb^{5+} ions at Zr^{4+} sites to form a Sr,Nb-rich layer, while Ca^{2+} will not form a Ca-rich layer because of its mismatch in ionic size and valence with Nb^{5+}. Thus, the gradual increase in the R_{gb} ratio in the Sr-LLZNb series with increasing Sr content is considered to result from the Sr,Nb-rich layer that becomes increasingly thick as the amount of Sr rises. These results also demonstrate that the solid solubility limit of Sr in LLZNb is apparently higher than that of Ca. In the case of Ca, the elemental concentration gradient seen with Sr was not observed, and the Ca and other elements were distributed evenly inside the grains. Even though Ca and Ca–Zr accumulations were found at grain boundaries, the grains were connected with

one another, which might have led to the low R_{gb} ratios in the Ca-LLZNb.

AUTHOR CONTRIBUTIONS

SO: conception and design of the study; YK: collection and assembly of data; TA: approval of this study.

ACKNOWLEDGMENTS

This study was partly supported by the project "Applied and Practical LiB Development for Automobile and Multiple Application" of the New Energy and Industrial Technology Development Organization (NEDO), Japan and Toyota Motor Corp.

REFERENCES

Allen, J. L., Wolfenstine, J., Rangasamy, E., and Sakamoto, J. (2012). Effect of substitution (Ta, Al, Ga) on the conductivity of Li7La3Zr2O12. *J. Power Sources* 206, 315–319. doi:10.1016/j.jpowsour.2012.01.131

Gao, X., Fisher, C. A. J., Kimura, T., Ikuhara, Y. H., Kuwabara, A., Moriwake, H., et al. (2014). Domain boundary structures in lanthanum lithium titanates. *J. Mater. Chem. A.* 2, 843–852. doi:10.1039/c3ta13726k

Inaguma, Y., Chen, L. Q., Itoh, M., Nakamura, T., Uchida, T., Ikuta, H., et al. (1993). High ionic-conductivity in lithium lanthanum titanate. *Solid State Commun.* 86, 689–693. doi:10.1016/0038-1098(93)90841-A

Jalem, R., Yamamoto, Y., Shiiba, H., Nakayama, M., Munakata, H., Kasuga, T., et al. (2013). Concerted migration mechanism in the Li ion dynamics of garnet-type Li7La3Zr2O12. *Chem. Mater.* 25, 425–430. doi:10.1021/cm303542x

Kihira, Y., Ohta, S., Imagawa, H., and Asaoka, T. (2013). Effect of simultaneous substitution of alkali earth metals and Nb in Li7La3Zr2O12 on lithium-ion conductivity. *ECS Electrochem. Lett.* 2, A56–A59. doi:10.1149/2.001307eel

Li, Y. T., Han, J. T., Wang, C. A., Xie, H., and Goodenough, J. B. (2012). Optimizing Li+ conductivity in a garnet framework. *J. Mater. Chem.* 22, 15357–15361. doi:10.1039/c2jm31413d

Logeat, A., Koohler, T., Eisele, U., Stiaszny, B., Harzer, A., Tovar, M., et al. (2012). From order to disorder: the structure of lithium-conducting garnets Li7-xLa3TaxZr2-xO12 (x=0-2). *Solid State Ionics.* 206, 33–38. doi:10.1016/j.ssi.2011.10.023

Moriwake, H., Gao, X., Kuwabara, A., Fisher, C. A. J., Kimura, T., Ikuhara, Y. H., et al. (2015). Domain boundaries and their influence on Li migration in solid-state electrolyte (La,Li)TiO3. *J. Power Sources* 276, 203–207. doi:10.1016/j.jpowsour.2014.11.139

Murugan, R., Thangadurai, V., and Weppner, W. (2007). Fast lithium ion conduction in garnet-type Li7La3Zr2O12. *Angew. Chem. Int. Ed.* 46, 7778–7781. doi:10.1002/anie.200701144

Nyman, M., Alam, T. M., McIntyre, S. K., Bleier, G. C., and Ingersoll, D. (2010). Alternative approach to increasing Li mobility in Li-La-Nb/Ta garnet electrolytes. *Chem. Mater.* 22, 5401–5410. doi:10.1021/cm101438x

Ohta, S., Kobayashi, T., and Asaoka, T. (2011). High lithium ionic conductivity in the garnet-type oxide Li7-X La-3(Zr2-X, Nb-X)O-12 (X=0-2). *J. Power Sources* 196, 3342–3345. doi:10.1016/j.jpowsour.2010.11.089

Ohtomo, T., Hayashi, A., Tatsumisago, M., and Kawamoto, K. (2013a). Suppression of H2S gas generation from the 75Li(2)S center dot 25P(2)S(5) glass electrolyte by additives. *J. Mater. Sci.* 48, 4137–4142. doi:10.1007/s10853-013-7226-8

Ohtomo, T., Hayashi, A., Tatsumisago, M., and Kawamoto, K. (2013b). Glass electrolytes with high ion conductivity and high chemical stability in the system LiI-Li2O-Li2S-P2S5. *Electrochemistery* 81, 428–431. doi:10.5796/electrochemistry.81.428

Rangasamy, E., Wolfenstine, J., Allen, J., and Sakamoto, J. (2013). The effect of 24c-site (A) cation substitution on the tetragonal-cubic phase transition in Li(7-x)La(3-x)A(x)Zr(2)O(12) garnet-based ceramic electrolyte. *J. Power Sources* 230, 261–266. doi:10.1016/j.jpowsour.2012.12.076

Shannon, R. D. (1976). Revised effective ionic radii and systematic studies of interatomic distances in halides and chalcogenides. *Acta Crystallograph. Sect. A* A32, 751–767. doi:10.1107/S0567739476001551

Stramare, S., Thangadurai, V., and Weppner, W. (2003). Lithium lanthanum titanates: are view. *Chem. Mater.* 15, 3974–3990. doi:10.1088/0953-8984/22/40/404203

Thompson, T., Wolfenstine, J., Allen, J. L., Johannes, M., Huq, A., David, I. N., et al. (2014). Tetragonal vs. cubic phase stability in Al – free Ta doped Li7La3Zr2O12 (LLZO). *J. Mater. Chem. A* 2, 13431–13436. doi:10.1039/c4ta02099e

Yashima, M., Itoh, M., Inaguma, Y., and Morii, Y. (2005). Crystal structure and diffusion path in the fast lithium-ion conductor La0.62Li0.16TiO3. *J. Am. Chem. Soc.* 127, 3491–3495. doi:10.1021/ja0449224

Conflict of Interest Statement: The authors declare that the research was conducted in the absence of any commercial or financial relationships that could be construed as a potential conflict of interest.